

Appearance-guided Attentive Self-Paced Learning for Unsupervised Salient Object Detection

Huajun Zhou, *Graduate Student Member, IEEE*, Bo Qiao, Lingxiao Yang, *Member, IEEE*
Jianhuang Lai, *Senior Member, IEEE*, Xiaohua Xie, *Member, IEEE*.

Abstract—Existing Deep-Learning-based (DL-based) Unsupervised Salient Object Detection (USOD) methods learn saliency information in images based on the prior knowledge of traditional saliency methods and pretrained deep networks. However, these methods employ a simple learning strategy to train deep networks and therefore cannot properly incorporate the “hidden” information of the training samples into the learning process. Moreover, appearance information, which is crucial for segmenting objects, is only used as post-process after the network training process. To address these two issues, we propose a novel appearance-guided attentive self-paced learning framework for unsupervised salient object detection. The proposed framework integrates both self-paced learning (SPL) and appearance guidance into a unified learning framework. Specifically, for the first issue, we propose an Attentive Self-Paced Learning (ASPL) paradigm that organizes the training samples in a meaningful order to excavate gradually more detailed saliency information. Our ASPL facilitates our framework capable of automatically producing soft attention weights that measure the learning difficulty of training samples in a purely self-learning way. For the second issue, we propose an Appearance Guidance Module (AGM), which formulates the local appearance contrast of each pixel as the probability of saliency boundary and finds the potential boundary of the target objects by maximizing the probability. Furthermore, we further extend our framework to other multi-modality SOD tasks by aggregating the appearance vectors of other modality data, such as depth map, thermal image or optical flow. Extensive experiments on RGB, RGB-D, RGB-T and video SOD benchmarks prove that our framework achieves state-of-the-art performance against existing USOD methods and is comparable to the latest supervised SOD methods. Code is available at www.github.com/moothes/A2S-v2.

Index Terms—Unsupervised learning, Salient object detection, Self-paced learning, Multi-modality.

I. INTRODUCTION

Unsupervised Salient Object Detection (USOD) aims to find the most conspicuous objects in images without manual annotation. USOD methods can be utilized as pre-process for other computer vision tasks, such as object recognition [1], [2], object detection [3], [4], and semantic segmentation [5], [6]. To produce more precise object masks, USOD methods are expected to correctly distinguish salient objects as well as their boundaries. However, natural images usually contain diverse objects, complex background, different lighting con-

The authors are with the School of Computer Science and Engineering, the Guangdong Province Key Laboratory of Information Security Technology, and the Key Laboratory of Machine Intelligence and Advanced Computing, Ministry of Education, Sun Yat-sen University, Guangzhou 510006, China (e-mail: zhouhj26@mail2.sysu.edu.cn; qiaob5@mail2.sysu.edu.cn; yanglx9@mail.sysu.edu.cn; xiexi-aoh6@mail.sysu.edu.cn; stsljh@mail.sysu.edu.cn).

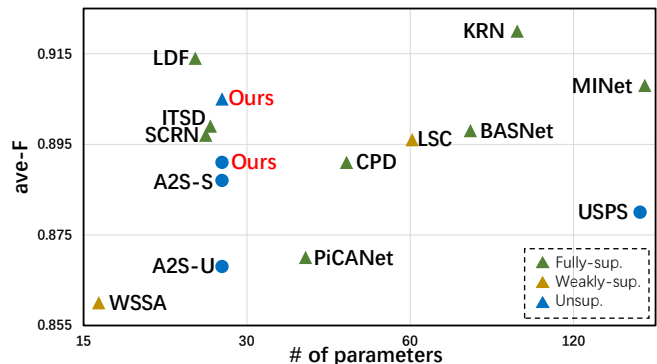


Fig. 1: Performance comparison between SOD methods. The circle and triangle indicate training on MSRA-B and DUTS-TR datasets, respectively.

ditions, and other challenging conditions, which bring severe challenges to detect salient objects in an unsupervised manner.

Recently, USOD methods have demonstrated impressive performance owing to the development of Deep-Learning techniques [7]–[9], as shown in Fig. 1. There are, however, mainly two limitations in these methods. First, unsupervised saliency modeling in images is not best served by current learning strategies. Specifically, most Deep-Learning-based (DL-based) USOD methods [10]–[13] learn image saliency based on noisy prior knowledge provided by several traditional SOD methods [14]–[17]. For example, USPS [12] uses the saliency cues extracted by traditional SOD methods to train deep networks in a fully-supervised manner. However, traditional SOD methods typically misidentify some background regions with distinctive colors as saliency regions, as shown in Fig. 2(c-d), because they model the image saliency using low-level features, such as color vectors. Using a simpler training strategy like USPS cannot effectively eliminate these regions (Fig. 2(e)), thus reducing the quality of pseudo labels. A2S [18] is able to eliminate these regions in the generated pseudo label (f-g) by modeling image saliency using high-level representations. However, a few patches in the generated pseudo labels are incorrectly classified, suggesting that some detailed saliency information has not yet been thoroughly uncovered. Second, there is still untapped potential for using appearance information to enhance segmentation performance. Existing DL-based USOD methods only use appearance information as post-process [19] to refine the network predictions. Although it refine the boundaries of target objects (Fig. 2 (e-h)), but is powerless when facing localization error in

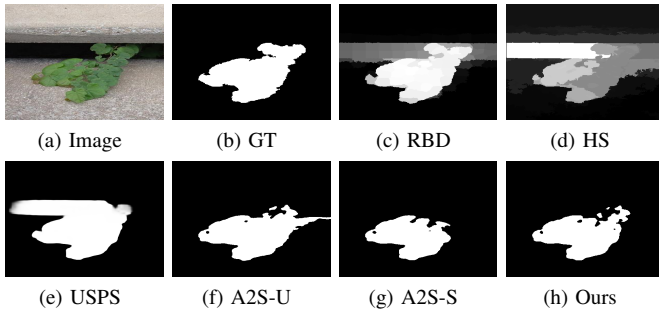


Fig. 2: Saliency maps generated by USOD methods. Two results of A2S are produced by using unsupervised (-U) and supervised (-S) encoders, respectively.

predictions. Instead, appearance information can be formulated as a supervision signal for deep networks to find more precise boundary of target objects during training. In summary, solving the above two issues is a promising direction to improve the performance of DL-based USOD methods.

For solving the first issue, we propose an effective way to formulate saliency modeling problem in an unsupervised fashion, which can better take advantage of weak saliency knowledge and gradually transfer them to more fine-level saliency labels. Actually, a robust learning strategy that can learn from subsets of high-confidence data and possibly avoid the chaos derived from the large amount of ambiguous data under such an unsupervised setting tends to be critical. This is because salient regions are always concealed inside many easily confused image regions in practical cases. Inspired by the self-paced learning (SPL) theory, we embed an Attentive Self-Paced Learning (ASPL) paradigm into our framework to alleviate the data ambiguity and guide a robust learning manner in complex scenarios. To gradually learn from the reliable training samples to the ambiguous ones, the original SPL model assigns a binary weight to each sample based on sample easiness and current training progress. Moreover, a sample regularizer is employed to learn more robust knowledge by increasing the sample diversity in learning. In this paper, we further leverage the sample easiness to simulate a continuous attention weight for each sample. Our weight generation process, like the original SPL, takes current training progress into account, which means that samples with the same easiness will acquire different weights at various stages of training. Our adaptive strategy leads to a more rational sample weighting scheme compared to the binary one as in SPL.

Concerning the second issue, we elucidate the natural relationship between object segmentation and pixel appearance information, and accordingly utilize the latter to facilitate low-level guidance for obtaining more precise object boundaries in the former problem. Specifically, intra-object consistency and boundary distinctiveness are two general characteristics of object appearance in the color image. This prior knowledge has been extensively studied in conventional non-learning segmentation methods [14], [17]. Many learning-based methods [34], [37] with a weakened supervision signal also use such prior to localize the boundaries of target objects. Specifi-

cally, by aligning the edges both in the color images and saliency predictions, they can produce high-quality boundary without using precise but expensive annotations. Such strategy bridges the connection between the appearance information and the supervision signal for training deep networks, like LSC [37]. However, knowledge learned from boundary pixels may be cancelled by other non-boundary pixels, resulting in a degraded segmentation performance. In our method, our framework can perceive coarse saliency regions by using the above ASPL paradigm that addresses the first issue. Most edges inside objects or the background have already been well settled, and therefore can be ignored in the proposed appearance guidance. By eliminating the effect of these pixels, our framework imposes more attention on refining boundaries using local appearance information. In addition, appearance information also can be interpreted as the feature vectors in other modalities, such as depth map, thermal image or optical flow. Our framework is capable of improving salient detection accuracy by aggregating multi-modality data.

Based on the above discussion, we propose a novel appearance-guided attentive self-paced learning framework for Unsupervised Salient Object Detection (USOD). By integrating the Self-Paced Learning (SPL) paradigm and the appearance guidance into a unified model, the proposed framework is capable of discovering the faithful and precise saliency patterns from the large number of ambiguous prior knowledge. Specifically, we propose an Attentive Self-Paced Learning (ASPL) paradigm as a more effective alternative to traditional SPL. Our ASPL introduces an adaptive weighting mechanism that assigns an attention factor for each sample conditioned on its current prediction and training progress. Furthermore, we propose an Appearance Guidance Module (AGM) to align the edges in both color images and saliency predictions, resulting in more robust segmentations in real complex scenarios. Benefit from the appearance information in multi-modality data, the proposed framework generates more precise saliency predictions in an unsupervised manner. Experiments on RGB, RGB-D, RGB-T and video SOD benchmarks prove that our framework achieves state-of-the-art performance against existing USOD methods and is comparable to the latest supervised SOD methods.

The main contributions are summarized as follows:

- 1) We propose an appearance-guided attentive self-paced learning framework for Unsupervised Salient Object Detection (USOD) by integrating both self-paced learning (SPL) and appearance guidance into a unified framework.
- 2) We propose an attentive self-paced learning paradigm that employs an adaptive weighting mechanism for training from simple samples to more complex ones conditioned on their current predictions and training progress.
- 3) We propose an Appearance Guidance Module (AGM) that leverages local low-level information to align the edges in color images and saliency predictions.
- 4) Experiments on RGB, RGB-D, RGB-T and video SOD benchmarks prove that our framework achieves state-of-the-art performance against existing USOD methods and is comparable to the latest supervised SOD methods.

II. RELATED WORKS

A. RGB Salient Object Detection

Supervised Methods. Researchers have developed a large family of fully-supervised Salient Object Detection (SOD) algorithms [20]–[27] in the past few years. Ronneberger et al. [28] proposed a U-shape structure that progressively upsamples and concatenates the smaller features to the larger ones. Zhang et al. [29] integrated multi-level features into a single feature, and used it to enhance the learned features. Hou et al. [30] introduced a weighted aggregation strategy to produce more precise predictions by fusing multi-level outputs. Qin et al. [31] proposed a novel loss function to supervise the network from pixel-, patch- and image-level simultaneously. Zhao et al. [32] developed a gate-based network to surpass the learned features in previous stages.

To ease the annotation burden, some researchers trained saliency detectors by using some low-cost annotations. Zeng et al. [33] used multi-source annotations to produce pseudo labels for unlabeled images. Piao et al. [34] employed several directive filters to synthesize more accurate saliency cues from multiple noisy pseudo labels. Zhang et al. [35] relabeled the DUTS-TR dataset [36] with scribbles and leveraged the edge detection task to tackle boundary localization. Yu et al. [37] proposed a local coherence loss to find precise boundary based on scribbles annotations. They employed all appearance information in images as guidance for training deep networks, where edges inside object or background may distract the learned saliency.

Although these methods have achieved significant performance, they train saliency detectors using numerous human annotations, which are very expensive to collect.

Unsupervised Methods. Existing DL-based USOD methods have proposed two pipelines to generate pseudo labels from images. First, most USOD methods [10]–[13], [38] focused on refining the coarse saliency cues extracted by several traditional SOD methods. For example, Zhang et al. [11] designed a noise modeling module to deal with noises in these saliency cues. Nguyen et al. [12] incrementally refine these saliency cues by using the self-supervision technique. Zhang et al. [38] proposed an encoder-decoder network to learn saliency information from these saliency cues. Second, to prevent the localization errors caused by traditional SOD methods, Zhou et al. [18] proposed a novel framework to extract high-quality saliency cues using a deep network. Although the above methods have achieved remarkable performance, there are two limitations in these methods. First, existing methods used a relatively simple training strategy to learned from all pixels in images, where reliable pixels and ambiguous pixels are coexisting. Second, low-level information, which is crucial for improving the segmentation performance, is utilized as post-process for network predictions.

In our work, we integrate self-paced learning and appearance guidance into a unified network. Specifically, we propose a attentive self-paced learning paradigm to better schedule the learning progress of our framework. Moreover, the appearance information is formulated as a supervision signal for obtaining precise object boundary.

B. Multi-modality Salient Object Detection

Multi-modality SOD means that using extra data from other modalities to improve the SOD performance, such as depth map, thermal image and optical flow.

Supervised Methods. To better integrate the auxiliary information, abundant methods were proposed recently [39]–[49]. Most of these methods employ a two-stream encoder-decoder structure to aggregate the appearance information from multi-modality data. To reduce the need of pixel-level annotations, Zhao et al. [50] proposed a VSOD dataset with scribbles to indicate the location of salient objects.

Similar to RGB SOD task, these methods still need extra efforts on annotating images, which is very laborious.

Unsupervised Methods. A few works focus on tackling multi-modality SOD task in an unsupervised manner. For example, Ji et al. [51] refined the saliency maps extracted by traditional SOD methods to produce more accurate saliency predictions. However, the same as RGB-based USOD methods, this method is sensitive to the quality of traditional SOD methods. Moreover, it has not well utilize appearance information during the network training process.

To the best of our knowledge, our work is the first in tackling various multi-modality Salient Object Detection (SOD) tasks by using a single unified framework. By modeling saliency information in images, our framework surpasses existing USOD methods and is comparable to the fully-supervised multi-modality SOD methods.

C. Self-Paced Learning

Learning from examples organized in a purposeful order that illustrates gradually more concepts is a natural learning process of humans and animals. Bengio et al. [52] proposed the self-paced (or curriculum) learning paradigm in response to this observation, in order to learn the model iteratively from simple to complex examples. To learn the model parameters \mathbf{w} and weight variable \mathbf{v} , the SPL minimizes:

$$\mathbb{E}(\mathbf{w}, \mathbf{v}; \lambda) = \sum_{i=1}^n v_i l(y_i, f(\mathbf{x}_i, \mathbf{w})) - \lambda \sum_{i=1}^n v_i, \quad (1)$$

$$s.t. \mathbf{v} \in [0, 1]^n,$$

where λ is a parameter for controlling the learning pace. The objective of SPL is to minimize the weighted training loss together with the negative l_1 -norm regularizer $-\|\mathbf{v}\|_1 = -\sum_{i=1}^n v_i$. In [53], [54], the ACS (Alternative Convex Search) is proposed to solve Eqn. 1 by using an iterative method for biconvex optimization. How to measure the easiness of samples is critical for the effectiveness of Self-Paced Learning (SPL). In original SPL, the easiness is estimated based on the loss term $l(y_i, f(\mathbf{x}_i, \mathbf{w}))$, where $f(\mathbf{x}_i, \mathbf{w}) = \phi_{\mathbf{w}}(\mathbf{x}_i)$. For example, Jiang et al. [55] assigned binary weights v for training samples to indicates whether they are taken into account in the training process. These weights are conditioned on the following principles: 1) samples with $l(y_i, \phi_{\mathbf{w}}(\mathbf{x}_i)) < T_l$ will be selected in training ($v_i = 1$); 2) samples with $l(y_i, \phi_{\mathbf{w}}(\mathbf{x}_i)) > T_h$ will not be selected in training ($v_i = 0$); 3) the weights for other samples will be decided by comparing

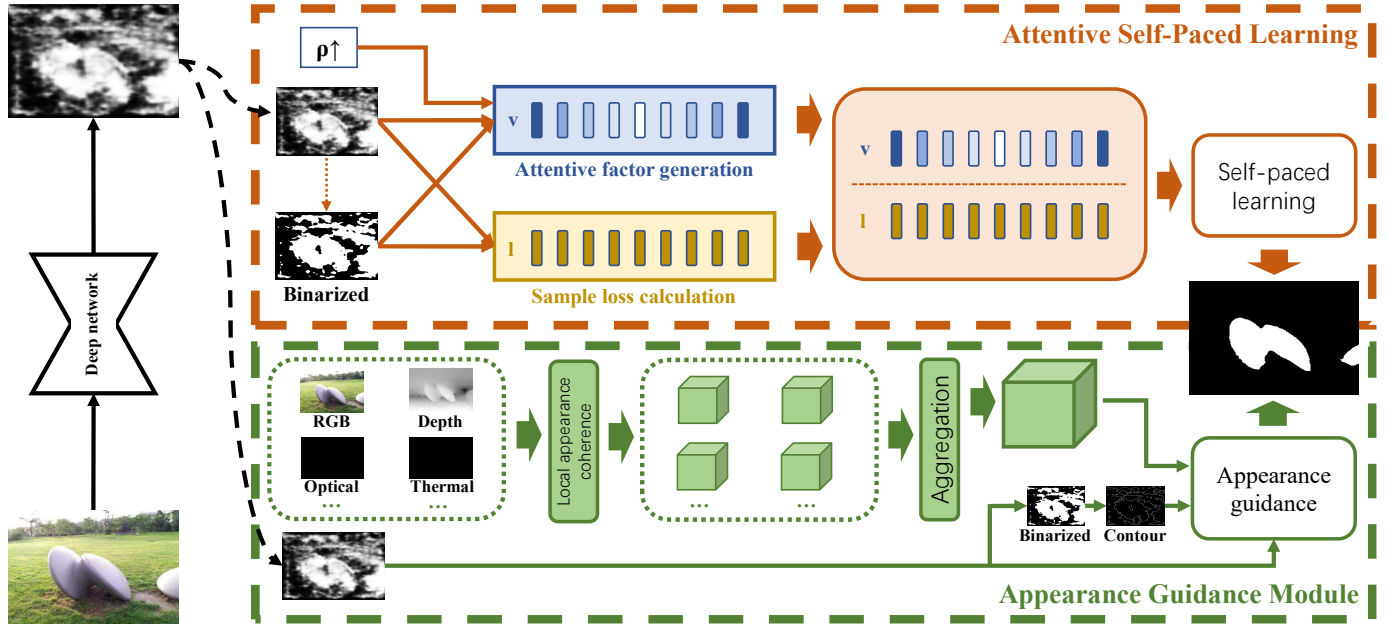


Fig. 3: Overview of our appearance-guided attentive self-paced learning framework. The network learns to produce high-quality saliency predictions from image in an unsupervised manner by using two novel supervision signals, Attentive Self-Paced Learning (ASPL) and Appearance Guidance Module (AGM). First, the ASPL paradigm promotes the network to excavate more detailed saliency information from simple samples to more difficult ones. Second, the AGM utilizes the appearance information from multi-modality data to refine the boundary of saliency predictions. We use a constant map to fill in the missing modalities of each image. The ρ is a parameter that gradually increases from 0 to 1 as the training progress.

their losses to the threshold $T_l + \frac{T_h}{\sqrt{i} + \sqrt{i+1}}$, where i is the sample's rank w.r.t. its loss value in group. T_l and T_h are hyperparameters and rise adaptively with the training process.

Such an intuitive learning strategy has been validated in a great deal of computer vision tasks. For example, Ghasedi et al. [56] proposed a balanced self-paced learning algorithm to adopt the generative adversarial network for clustering. Soviany et al. [57] leveraged SPL to tackle cross-domain object detection by progressively learning unlabeled samples in target domains. Zhu et al. [58] tackled the spectrum reconstruction by using SPL to select the training samples in each iteration. Zhang et al. [59] integrated multiple-instance learning and SPL into a unified network to address co-saliency detection.

In this paper, we adapt the SPL paradigm to the USOD task based on the specific sample distributions. Moreover, we build an adaptive weighting mechanism for all samples conditioned on current predictions and training progress.

III. OUR APPROACH

A. Framework Overview

Graphical illustration of the proposed framework is shown in Fig. 3. First, we propose an Attentive Self-Paced Learning (ASPL) paradigm to excavate finer saliency knowledge gradually from simple examples to the complex ones. Second, we propose an Appearance Guidance Module (AGM) to formulate the local appearance contrast of each pixel as the probability of saliency boundary and finds the potential boundary of the target objects by maximizing the probability. In addition, multi-scale training is employed during training and we ensure

the scale consistency using a L2 loss L_{ms} . Overall, the loss function used to train our framework is:

$$L_{s1} = \lambda_s L_{aspl} + \lambda_s \hat{L}_{aspl} + \lambda_a L_{agm} + \lambda_a \hat{L}_{agm} + \lambda_m L_{ms}, \quad (2)$$

where all λ are hyperparameters. The \hat{L} indicates the loss for the predictions of a reference scale.

B. Attentive Self-Paced Learning

A prerequisite of conventional SPL is that all labels for samples are known beforehand. In this case, assigning different weights for samples may vary the gradients but still along to the optimal. However, for USOD, our initial labels for each pixels are noisy. Learning from partial ambiguous pixels are prone to distract the learned saliency modeling patterns in deep networks, resulting in a weakened detection performance. To address this issue, the proposed ASPL employs soft weights to aggregate saliency information from all samples for modeling more accurate saliency patterns in images. Moreover, our ASPL employs a dynamic weighting strategy conditioned on the current learning process to learn from easy samples to the complex ones.

To learn saliency in images, our ASPL paradigm approximates the distribution of saliency predictions to an ideal distribution. Specifically, in the ideal case, the SOD results follow a Bernoulli distribution. While in practice, the saliency prediction of our network follows a continuous distribution. Such a continuous distribution can be considered as a combination of a clean Bernoulli distribution and random noise. By driving the network predictions to converge to a Bernoulli distribution, we

can recover more accurate saliency information. In our ASPL, we use the L1 loss to reducing the distance for each pixel to its potential label by:

$$l(\tilde{y}_i, \phi_{\mathbf{w}}(\mathbf{x}_i)) = |\tilde{y}_i - \phi_{\mathbf{w}}(\mathbf{x}_i)| \Leftrightarrow -|\phi_{\mathbf{w}}(\mathbf{x}_i) - 0.5|, \quad (3)$$

where \tilde{y}_i is the potential label, which is defined as:

$$\tilde{y}_i = \begin{cases} 1, & \text{if } \phi_{\mathbf{w}}(\mathbf{x}_i) > 0.5; \\ 0, & \text{if } \phi_{\mathbf{w}}(\mathbf{x}_i) \leq 0.5. \end{cases} \quad (4)$$

Minimizing the distance between predictions and potential labels by $|\tilde{y}_i - \phi_{\mathbf{w}}(\mathbf{x}_i)|$ is equivalent to maximize $|\phi_{\mathbf{w}}(\mathbf{x}_i) - 0.5|$, where 0.5 is the center between two classes, 0 and 1.

How to formulate the weights of samples is critical for the effectiveness of the SPL-based paradigms. Intuitively, pixels closed to target distribution are easy samples and contains more reliable saliency information. Learning from these pixels can conclude some general saliency patterns in images. For other pixels of greater difficulty, saliency information is hidden within noise. A sophisticated training strategy is required to reveal the hidden saliency information in such noisy pixels. At the beginning of the training phase, we assign high weights to the easy samples to learn more reliable saliency information and reduce interest in difficult samples to prevent noise from interfering with the learned saliency patterns. Since the network has learned reliable saliency patterns as the training process progresses, we can gradually increase the weights of difficult samples to uncover more detailed saliency information while having little effect on the patterns already learned. Based on the above analysis, the weight v in ASPL is defined as:

$$v_i = |\phi_{\mathbf{w}}(\mathbf{x}_i) - 0.5|^{(2^{1-\rho}-1)}, \quad (5)$$

where ρ is a parameter that increases linearly from 0 to 1 with the training process. As for the regularizer term in the Eqn. 1, its aim is to increase the number of samples involved in the training of the model. This item is removed in our ASPL because all samples contribute to the training process to varying degrees.

Finally, the overall loss function of our ASPL can be summarized as:

$$L_{aspl} = \sum_{i=1}^n v_i l(y_i, f(\mathbf{x}_i, \mathbf{w})) = -|\phi_{\mathbf{w}}(\mathbf{x}_i) - 0.5|^{(2^{1-\rho})}, \quad (6)$$

The partial derivative of our L_{aspl} over $k_i = \phi_{\mathbf{w}}(\mathbf{x}_i) - 0.5$ is

$$\frac{\partial L_{aspl}}{\partial k_i} = -\text{sign}(k_i) 2^{(1-\rho)} |k_i|^{2^{(1-\rho)}-1}, \quad (7)$$

where $\text{sign}(k_i) \in [-1, 1]$. The gradient curves of $\frac{\partial L_{aspl}}{\partial k_i}$ for different $|k_i|$ are visualized in Fig. 4(b). For pixels with small $|k_i|$, their gradients increase quickly during the training process. While the gradients of pixels with large $|k_i|$ are relative stable for the whole training process. In this way, our ASPL guides our saliency generator to extract coarse-to-fine saliency cues from images by dynamically shifting its attention from easy samples to more complex ones.

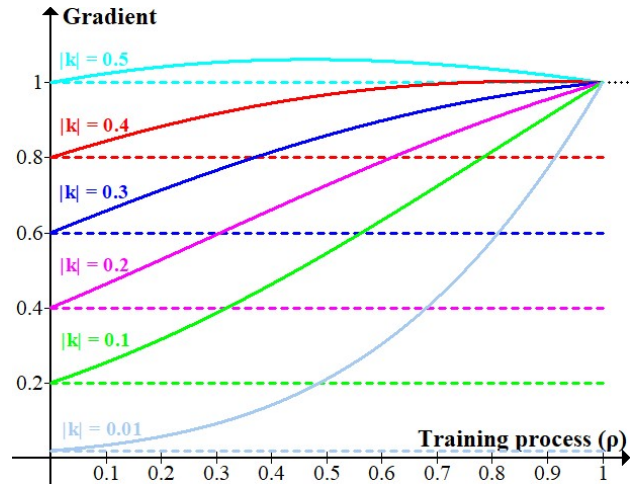


Fig. 4: Gradient comparison between ADB [18] and our ASPL losses. The solid and dotted lines are gradient curves for L_{aspl} and L_{adb} , respectively.

C. Appearance Guidance Module

Appearance information is essential for distinguishing between object boundaries and surrounding background. For example, many traditional segmentation methods [60]–[62] used this information to generate precise boundaries for target objects. Inspired by these works, we propose a Appearance Guidance Module (AGM) to reduce the saliency differences between a neighborhood of a given pixel. As shown in Fig. 5, our AGM bridges the correlation between saliency prediction and appearance information by multiplying three terms:

$$L_{agm} = \sum_i \sum_{j \in K_i} b_i s_{i,j} d_{i,j}, \quad (8)$$

where b_i and K_i is the boundary mask and 11×11 neighbors of i -th pixel, respectively. First, we introduce a boundary mask into our AGM to avoid the negative effects caused by internal edges in the background or objects. The boundary masks are generated by using two 5×5 max-pooling operations on our saliency predictions:

$$B = \text{maxpool}(Y) * \text{maxpool}(1 - Y), \quad (9)$$

where Y and B are the predicted saliency maps and corresponding boundary masks, respectively. The b_i is the pixel sample in B . Second, the saliency difference is measured using L1 distance:

$$s_{i,j} = |y_i - y_j|, \quad (10)$$

where y_i is the i -th pixel in Y , while y_j is a neighbor pixel around y_i . Third, for pixels close to an object boundary, their appearances are often different from surrounding pixels. An exponential distance is employed to measure the appearance similarity by:

$$d_{i,j} = \exp(-\alpha \|\mathbf{x}_i - \mathbf{x}_j\|^2), \quad (11)$$

where \mathbf{x} is a color vector and $\|\cdot\|^2$ is the Euclidean distance. α is a hyperparameter that controls the effect of appearance similarity.

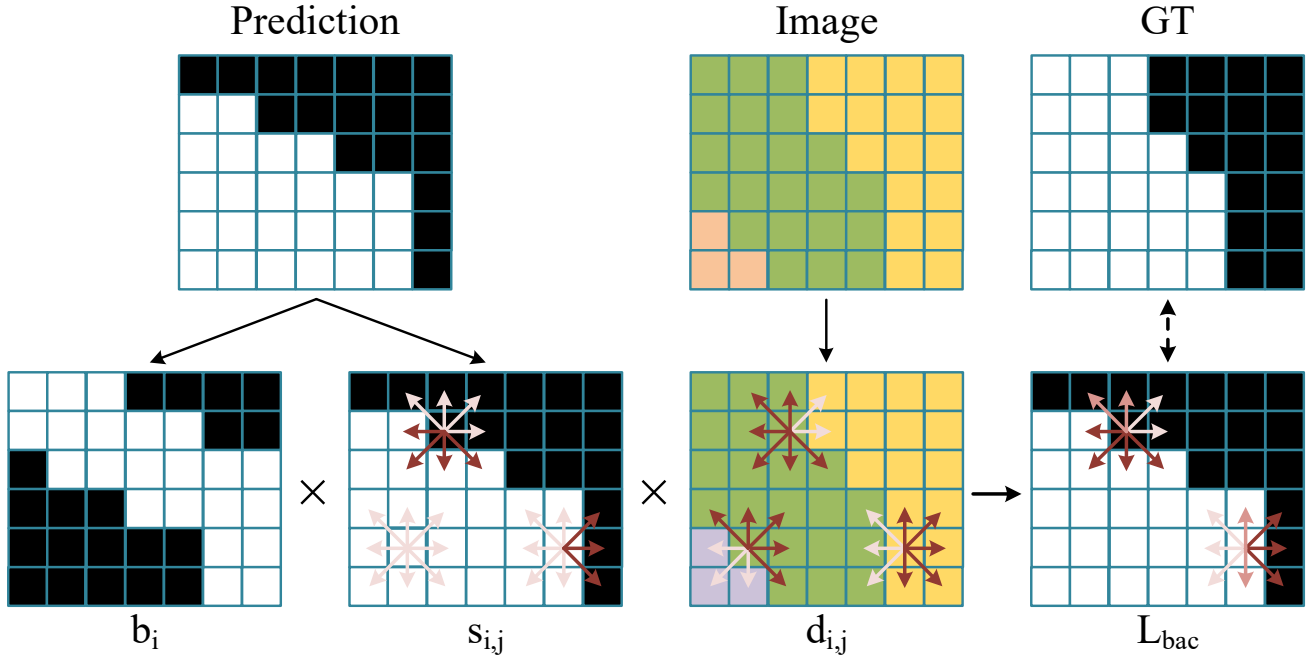


Fig. 5: Graphical illustration of L_{agm} . Our L_{agm} consists of three terms: boundary mask b_i , saliency difference $s_{i,j}$, and appearance similarity $d_{i,j}$. Arrows with deep colors indicate large values. We select three pixels as examples. The topmost example tends to be salient, as most neighbors with similar appearances are salient. Bottomleft example is eliminated because it is the internal edge of salient object.

From a broader perspective, appearance also can be interpreted as features in other modality data, such as depth map, optical flow and thermal image. For salient regions that are not distinctive to surrounding background pixels in color image, they may be distinctive in other modality data. Therefore, integrating the appearance information in multi-modality data can improve the segmentation accuracy. Defining $X^m, m \in [1, M]$ as the data from the m -th modality, we re-formulate the appearance similarity defined in Eqn. 11 as:

$$d_{i,j} = \exp(-\alpha \sum_{m=1}^M \|\mathbf{x}_i^m - \mathbf{x}_j^m\|^2), \quad (12)$$

where \mathbf{x}_i^m is the i -th feature from m -th modality. However, in practical scenarios, it is extremely hard to collect all multi-modality data for the same image. To tackle the missing modality data, we can simply embed a constant map to our framework. In this case, $\|\mathbf{x}_i^m - \mathbf{x}_j^m\|^2 = 0$ will not affect the calculation of appearance similarity.

D. Multi-scale Training

Salient objects are consistent for the same images of different scales. Therefore, we resize input images to a reference scale and encourage our network to produce consistent predictions for multi-scale inputs. The predictions \hat{p} of reference scale are resized to the original size and compute its difference with p by:

$$L_{ms} = \sum_i |y_i - \text{resize}(\hat{y}_i)|^2. \quad (13)$$

where y_i and \hat{y}_i are saliency predictions in original and reference scales, respectively.

E. Network Construction.

We build a simple network ϕ to produce one-channel predictions for each image, which is defined as:

$$\phi(X) = Y, \quad (14)$$

where X and Y are input image and prediction, respectively. Following previous method [18], our network consists of an ImageNet pre-trained encoder and several Squeeze-and-Excitation (SE) blocks. The formulas of our network ϕ are shown as follows:

$$\begin{aligned} E_3, E_4, E_5 &= \text{Encoder}(X), \\ F_i &= \text{SE}(E_i), i = 3, 4, 5, \\ H &= \text{SE}(\text{concat}(F_3, F_4, F_5)), \\ Y &= \text{Sigmoid}(\text{sum}(H - \bar{H})), \end{aligned} \quad (15)$$

where \bar{H} is the global mean of H . Specifically, our encoder is instantiated as the ResNet-50 [7] pretrained by MoCo-v2 [63], which does not require any human annotation for training. We select the features from stage 3 to 5 of the encoder to modeling saliency because they have concluded more global statistics, which are crucial for localizing salient objects. We further reduce the channel of each feature to 64 and reorganize its learned knowledge using an SE block. Subsequently, an additional SE block is employed to integrate the knowledge of all three features after concatenation, denoted as H . After that, H is subtracted by its global mean to ensure the coexisting of positive and negative samples, and summed over the channel dimension to produce one-channel predictions. Finally, a Sigmoid function is appended to produce the preliminary saliency predictions.

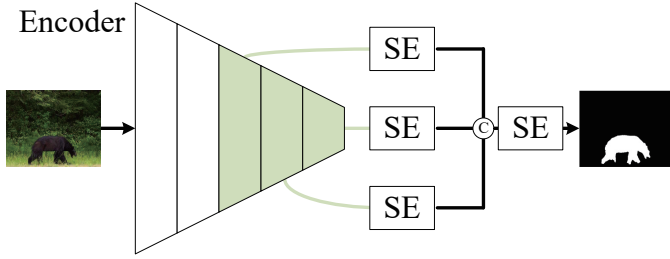


Fig. 6: The network structure used in our framework.

F. Training a Generalized Detector

Our framework can produce high-quality saliency predictions for training samples by modeling intrinsic knowledge in the visible images. However, during testing, it may not work well for the unseen images without fine-tuning based on the intrinsic knowledge. Therefore, following previous methods [10], [12], we employ a second stage to train a generalized saliency detector using the pseudo labels generated by our framework. The saliency detector can be any existing fully-supervised SOD network. IOU loss is employed as the loss function for training the detector:

$$L_{s2} = L_{iou}(P, \check{Y}) = 1 - \frac{\text{sum}(P * \check{Y})}{\text{sum}(P + \check{Y} - P * \check{Y})}, \quad (16)$$

$$\check{Y} = \text{CRF}(Y)$$

where P and Y are the prediction of detector and our pseudo labels, respectively.

IV. EXPERIMENTS

A. Experiment settings

Setup. All experiments are implemented on a single GTX 1080 Ti GPU using PyTorch [64]. The batch size is 8 and images are resized to 320^2 . The reference scale in multi-scale training is randomly selected from $(192^2, 256^2, 384^2, 448^2)$. For data augmentation, horizontal flipping is employed during the training process. SGD is utilized as the optimizer to train our framework for 20 epochs. The initial learning rate is set to 0.1 and decayed using a linear schedule. In addition, α in Eqn. 11 is set to 200. Meanwhile, λ_d , λ_b and λ_m in Eqn. 2 are set to 1, 0.05 and 1, respectively. In the generalized salient object detection phase, we use a learning rate of 0.005 to train our saliency detector for 10 epochs. For RGB SOD, the same network as previous method [18] is trained on the generated pseudo labels. For multi-modality SOD tasks, we use the generated pseudo labels to train the MIDD [49] network. Noted that all networks in our framework use MoCo-v2 pretrained ResNet-50 as backbone to ensure that no manual labels are involved in the whole training process.

Datasets. To make a fair comparison with existing SOD methods, we train our framework on the train subsets of MSRA-B [65] or DUTS [36] datasets separately. ECSSD [66], PASCAL-S [67], HKU-IS [68], DUTS-TE [36], DUT-O [69] as well as the test subset of MSRA-B are employed to evaluate the performance of the proposed framework. They have 1000, 850, 4447, 5019, 5168, and 2000 images, respectively.

For multi-modality SOD tasks, including RGB-D, RGB-T and video SOD, we use the same datasets as existing fully-supervised methods [47], [51], [70]. Specifically, for RGB-D SOD, we choose the same 700 samples from NLPR [71] and 1485 samples from NJUD [72] to train our framework. Our method is evaluated on RGBD135 [73], NJUD, NLPR and SIP [74], which contain 135, 500, 300 and 929 images, respectively. For RGB-T SOD, we choose the same 2500 images in VT5000 [75] as our train set, while the rest 2500 images in VT5000, 1000 images in VT1000 [76] and 821 images in VT821 [77] are employed as the test sets. For video SOD, we choose the train splits of DAVIS [78] and DAVSOD [40] to train our framework. Due to the high sample rate of DAVSOD, we randomly sample 5 frames of each video to avoid overfitting. Moreover, the test splits of DAVIS, DAVSOD, SegV2 [79] and FBMS [80] are employed as the test sets, which contains 1376, 5332, 1025 and 367 images, respectively.

Metrics. We adopt three criteria in our experiments, including ave- F_β , Mean Absolute Error (MAE) and Enhanced-alignment Measure (E_ξ). F_β is computed by:

$$F_\beta = \frac{(1 + \beta^2) \times \text{Precision} \times \text{Recall}}{\beta^2 \times \text{Precision} + \text{Recall}}, \quad (17)$$

where β^2 is set to 0.3 [93] in general. The ave- F_β is the F_β scores by setting the threshold as two times average value of the predictions. In addition, MAE is calculated by:

$$\mathcal{M} = \frac{1}{W \times H} \sum_{i=1}^W \sum_{j=1}^H |p_i - g_i|, \quad (18)$$

where p_i and g_i are prediction and ground truth, respectively. Enhanced-alignment Measure (E_ξ) [94] captures global statistics and local pixel matching information by:

$$E_\xi = \frac{1}{W \times H} \sum_{i=1}^W \sum_{j=1}^H \phi(i, j), \quad (19)$$

where $\phi(i, j)$ is the enhanced alignment matrix.

B. Results on RGB SOD

We compare the proposed framework with **fully-supervised** methods, PiCANet [20], BASNet [31], CPD [21], SCRNet [81], ITSD [82], MINet [83], LDF [84], and KRN [85], **weakly-supervised** methods, WSS [86], ASMO [87], MSW [33], WSSA [35], MFNet [34], and SCW [37], and **unsupervised** methods, SBF [10], MNL [11], USPS [12], EDNS [38], A2S [18], and DCFD [13]. The results of these methods on six SOD benchmarks are exhibited in Tab. I.

Either training on MSRA-B or DUTS-TR, the proposed framework achieves significant improvements compared to existing USOD methods. These results prove the effectiveness and generalization ability of the proposed framework. Compared to weakly-supervised SOD methods, our unsupervised framework still surpasses most of them and achieves similar results to state-of-the-art SCW [37] method. It proves that modeling multi-level representations of images can produce

TABLE I: Experiment results on SOD benchmarks. ‘‘E&S’’ indicates the supervised signals used to train encoders and SOD methods. ‘‘F’’, ‘‘W’’ and ‘‘U’’ mean fully-supervised, weakly-supervised and unsupervised, respectively. Best scores are in bold.

Methods	Year	E&S	ECSSD			MSRA-B			DUT-O			PASCAL-S			DUTS-TE			HKU-IS		
			$F_{\beta}\uparrow$	$E_{\xi}\uparrow$	$M\downarrow$	$F_{\beta}\uparrow$	$E_{\xi}\uparrow$	$M\downarrow$	$F_{\beta}\uparrow$	$E_{\xi}\uparrow$	$M\downarrow$	$F_{\beta}\uparrow$	$E_{\xi}\uparrow$	$M\downarrow$	$F_{\beta}\uparrow$	$E_{\xi}\uparrow$	$M\downarrow$	$F_{\beta}\uparrow$	$E_{\xi}\uparrow$	$M\downarrow$
Trained on DUTS-TR																				
PiCANet [20]	2018	F&F	.886	.927	.046	.874	.933	.055	.717	.848	.065	.804	.862	.076	.759	.873	.051	.870	.941	.044
BASNet [31]	2019	F&F	.879	.921	.037	.896	.942	.036	.756	.869	.056	.781	.853	.077	.791	.884	.048	.898	.947	.033
CPD [21]	2019	F&F	.917	.949	.037	.899	.947	.038	.747	.873	.056	.831	.887	.072	.805	.904	.043	.891	.952	.034
SCRN [81]	2019	F&F	.918	.942	.037	.868	.929	.063	.746	.869	.056	.839	.888	.065	.809	.901	.040	.897	.954	.033
ITSD [82]	2020	F&F	.905	.933	.035	.902	.948	.038	.750	.863	.059	.817	.868	.066	.808	.897	.040	.899	.953	.030
MINet [83]	2020	F&F	.924	.953	.033	.903	.948	.038	.756	.873	.055	.842	.899	.064	.828	.917	.037	.908	.961	.028
LDF [84]	2020	F&F	.930	.951	.034	.902	.944	.037	.773	.881	.052	.853	.903	.062	.855	.929	.034	.914	.960	.028
KRN [85]	2021	F&F	.931	.951	.032	.911	.950	.036	.793	.893	.050	.851	.894	.068	.865	.934	.033	.920	.961	.027
WSS [86]	2017	F&W	.767	.769	.108	–	–	–	.590	.729	.110	.698	.690	.184	.633	.806	.100	.773	.819	.079
ASMO [87]	2018	F&W	.762	.792	.068	–	–	–	.641	.761	.100	.653	.647	.206	.569	.690	.116	.763	.800	.089
MSW [33]	2019	F&W	.761	.788	.098	.861	.924	.073	.597	.728	.109	.685	.693	.178	.648	.742	.091	.734	.786	.084
WSSA [35]	2020	F&W	.870	.917	.059	.869	.929	.049	.703	.845	.068	.785	.855	.096	.742	.869	.062	.860	.932	.047
MFNet [34]	2021	F&W	.844	.889	.084	.872	.923	.059	.621	.784	.098	.756	.824	.115	.693	.832	.079	.839	.919	.058
SCW [37]	2021	F&W	.900	.931	.049	.898	.940	.040	.758	.862	.060	.827	.879	.080	.823	.890	.049	.896	.943	.038
EDNS [38]	2020	F&U	.872	.906	.068	.880	.932	.051	.682	.821	.076	.801	.846	.097	.735	.847	.065	.874	.933	.046
DCFD [13]	2022	F&U	.888	.915	.059	.888	.930	.045	.710	.837	.070	.795	.860	.090	.764	.855	.064	.889	.935	.042
Ours	2022	U&U	.916	.938	.044	.904	.944	.039	.745	.863	.061	.830	.882	.074	.810	.901	.047	.902	.947	.037
Trained on MSRA-B																				
SBF [10]	2017	F&U	.812	.878	.087	.867	.929	.058	.611	.771	.106	.711	.795	.131	.627	.785	.105	.805	.895	.074
MNL [11]	2018	F&U	.874	.906	.069	.881	.932	.053	.683	.821	.076	.792	.846	.091	–	–	–	.874	.932	.047
USPS [12]	2019	F&U	.875	.903	.064	.896	.938	.042	.715	.839	.069	.770	.828	.107	.730	.840	.072	.880	.933	.043
A2S [18]	2021	F&U	.888	.911	.064	.902	.941	.041	.719	.841	.069	.790	.838	.106	.750	.860	.065	.887	.937	.042
DCFD [13]	2022	F&U	.880	.900	.064	.903	.938	.041	.731	.838	.064	.773	.830	.105	.744	.832	.068	.887	.926	.044
A2S [18]	2021	U&U	.882	.921	.056	.886	.939	.041	.688	.818	.079	.778	.842	.100	.729	.847	.069	.868	.936	.041
Ours	2022	U&U	.902	.923	.056	.912	.948	.036	.731	.851	.065	.803	.848	.099	.767	.871	.061	.891	.939	.041

TABLE II: Setting comparison among USOD methods. Note that some methods exclude the time for extracting saliency cues using traditional methods. ‘‘F’’ and ‘‘U’’ indicate fully-supervised and unsupervised training strategies. ‘‘IN’’ and ‘‘CS’’ are ImageNet [9] and CityScape [8] datasets, respectively.

Method	Train set	Input	Encoder	Pretrain	Saliency cues	Train time
EDNS [38]	DUTS-TR	352×352	VGG-16	F-IN	[16], [88], [89]	>8h
DCFD [13]	DUTS-TR	–	ResNet-50	F-IN	[15]	–
Ours	DUTS-TR	320×320	ResNet-50	U-IN	No	4.5h
SBF [10]	MSRA-B	224×224	VGG-16	F-IN	[90]–[92]	>3h
MNL [11]	MSRA-B	425×425	ResNet-101	F-IN	[15]–[17], [92]	>4h
USPS [12]	MSRA-B	432×432	ResNet-101	F-CS	[15]–[17], [92]	>30h
DCFD [13]	MSRA-B	–	ResNet-101	F-CS	[15]	–
A2S [18]	MSRA-B	320×320	ResNet-50	U-IN	No	1h
Ours	MSRA-B	320×320	ResNet-50	U-IN	No	1.3h

more precise saliency information than low-cost human annotations. In addition, the performance of our framework is comparable to the latest fully-supervised SOD methods. These results imply that unsupervised USOD methods have the potential to achieve more competitive performance against fully-supervised SOD methods. It conveys an encouraging message that human annotation may not be required for training a robust saliency detector.

Based on the setting comparison between USOD methods in Tab. II, we have the following conclusions. First, the proposed framework achieves better performance than other methods under more disadvantaged settings, *e.g.*, smaller input size, and weakened encoders. Second, the latest MNL [11], USPS [12] and DCFD [13] use ResNet-101 [7] as encoder, which is more powerful than our ResNet-50. Moreover, their encoders are pretrained using image- or pixel-level labels, while our encoder is pretrained without using any human annotation. Third, no human annotation is involved in the training process of our framework, including the pretraining of encoders. Fourth, similar to A2S [18], our framework does not rely on any

traditional SOD method to extract coarse saliency cues from images. Last, training efficiency of our framework is much higher than most USOD methods. A2S is slightly faster than us, but its performance is significantly lower.

A qualitative comparison of SOD methods on several challenging cases is illustrated in Fig. 7. First, our framework better differentiates salient objects with surrounding backgrounds and produces distinct boundaries than existing USOD methods. For example, in the first image, multiple SOD methods fail to capture the tiny salient object. Our framework and two fully-supervised SOD methods well segment this object with precise boundaries. Second, as shown in the sixth example, existing USOD methods are struggling to capture entire salient objects. On the contrary, the proposed framework well captures entire salient objects as fully-supervised methods. Last, our framework can produce more clean background than other methods. In the last image, most SOD methods consider those characters may be salient because of their similar colors with the dog. Our saliency prediction is much more distinct than these methods.

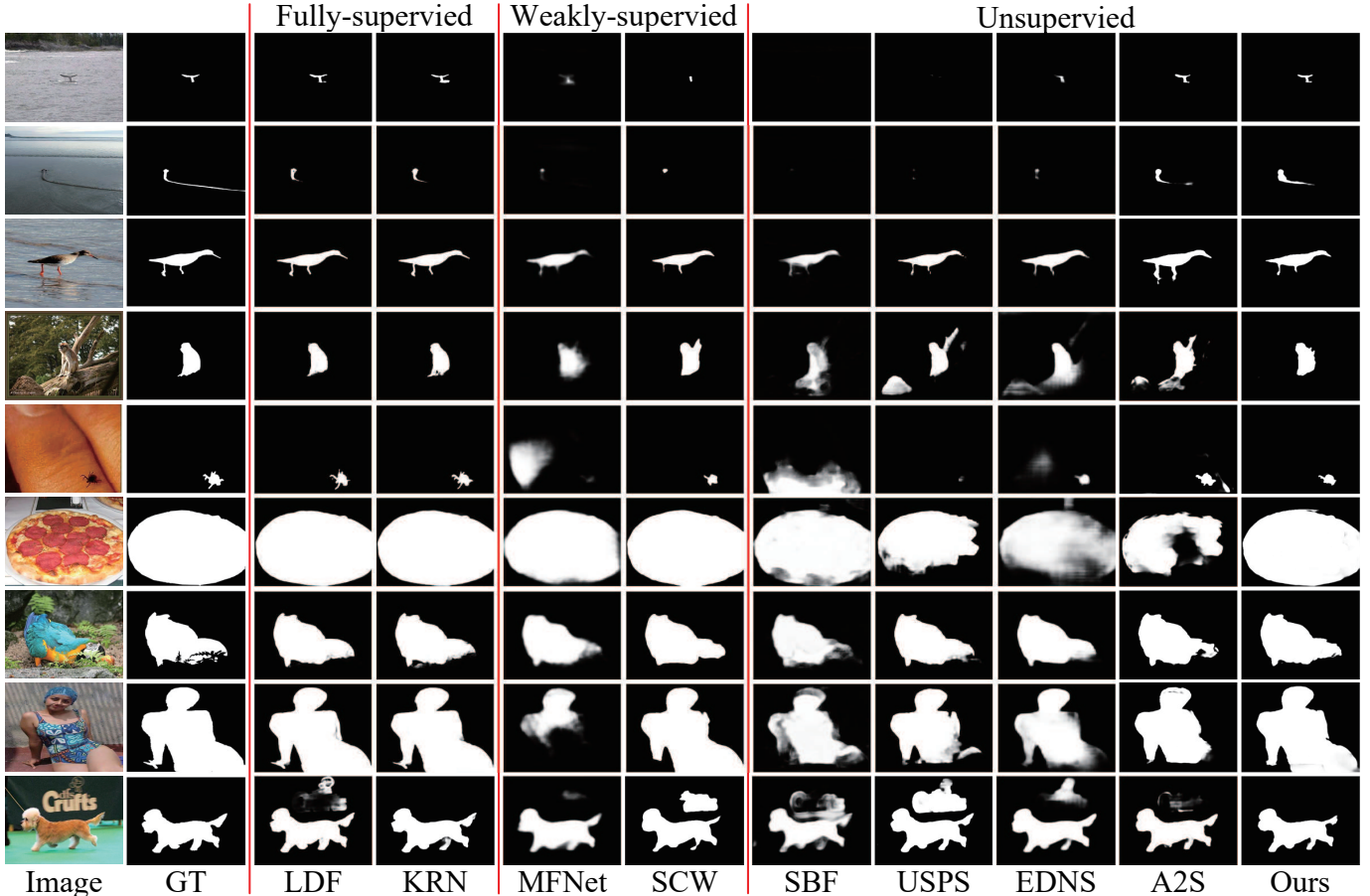


Fig. 7: Visual comparison with state-of-the-art SOD methods.

TABLE III: The quality of pseudo labels for multi-modality SOD datasets.

Training data	RGB			RGB-D			VSOD			RGB-T		
	$F_{\beta}\uparrow$	$E_{\xi}\uparrow$	$M\downarrow$	$F_{\beta}\uparrow$	$E_{\xi}\uparrow$	$M\downarrow$	$F_{\beta}\uparrow$	$E_{\xi}\uparrow$	$M\downarrow$	$F_{\beta}\uparrow$	$E_{\xi}\uparrow$	$M\downarrow$
MM-split	.917	.945	.038	.672	.693	.135	.557	.725	.099	.932	.951	.029
Only-RGB	.917	.941	.040	.804	.874	.068	.613	.784	.089	.920	.950	.030
MM-joint	.918	.941	.040	.826	.892	.062	.637	.805	.079	.923	.952	.029

C. Results on Multi-modality SOD

To validate the generalization ability of the proposed framework, we conduct more experiments on multi-modality SOD tasks, including RGB-D, RGB-T and video. Noted that for the video SOD task, we pre-compute the optical flow for each frame as an extra modality data. Since there are different modality data, we train our framework under three sets of data: 1) *Task-specific multi-modality data* (“MM-split”). For example, for RGB-T SOD task, we only use 2500 RGB-thermal image pairs to train our framework. Other multi-modality SOD tasks follow a similar setting. 2) *RGB images from all tasks* (“Only-RGB”). 3) *All multi-modality data from all tasks* (“MM-joint”). In Tab. III, we show the scores of saliency predictions on corresponding training sets.

Overall, training on the union set of all multi-modality data (“MM-joint”) reports a more generalized performance on all datasets. An interesting observation is that training on task-specific data (“MM-split”) obtains slightly better performance on RGB and RGB-T datasets, while is significantly inferior on

RGB-D and VSOD datasets. Under the unsupervised setting, training on all multi-modality data may report slightly worse performance on a subset of training set to learn more generalized saliency information from other data. Meanwhile, due to a low diversity of data in RGB-D and VSOD dataset, training on such data is prone to focus on some discriminative regions of target objects, as shown in Fig. 8. In addition, the results on “Only-RGB” prove that multi-modality data can guide our framework to learn more accurate saliency information.

The above experiments provide a quantitative validation on the quality of pseudo labels produced by using different training data. For a more intuitive illustration, we employ these pseudo labels of task-specific dataset to train a task-specific saliency detector like conventional fully-supervised methods. For the RGB-D SOD task in Tab. IV, using the labels of “MM-split” can obtain slightly better performance than the recently proposed unsupervised RGB-D SOD method DSU [51]. Moreover, using the labels of “MM-joint” can achieve a competitive performance against the latest fully-

TABLE IV: Results on RGB-D SOD datasets. “F” and “U” mean fully-supervised and unsupervised, respectively.

Methods	Year	Sup.	RGBD135			NJUD			NLPR			SIP		
			$F_{\beta}\uparrow$	$E_{\xi}\uparrow$	$\mathcal{M}\downarrow$	$F_{\beta}\uparrow$	$E_{\xi}\uparrow$	$\mathcal{M}\downarrow$	$F_{\beta}\uparrow$	$E_{\xi}\uparrow$	$\mathcal{M}\downarrow$	$F_{\beta}\uparrow$	$E_{\xi}\uparrow$	$\mathcal{M}\downarrow$
DSNet [39]	2021	F	.899	.969	.020	–	–	–	.886	.957	.024	.864	.920	.052
DSA2F [42]	2021	F	.899	.958	.021	.901	.937	.039	.897	.953	.024	–	–	–
SPNet [43]	2021	F	.927	.984	.013	–	–	–	.903	.959	.021	.893	.931	.043
DIGR [44]	2022	F	.898	.969	.019	–	–	–	.889	.956	.023	.878	.918	.053
CCFE [70]	2022	F	.911	.964	.020	.914	.953	.032	.907	.962	.021	.889	.923	.047
DSU [51]	2022	U	.767	.895	.061	.719	.797	.135	.745	.879	.065	.619	.774	.156
MM-split (Ours)	2022	U	.845	.910	.051	.709	.722	.148	.836	.903	.055	.650	.677	.151
MM-joint (Ours)	2022	U	.877	.946	.029	.862	.908	.060	.852	.931	.034	.873	.925	.051

TABLE V: Results on VSOD datasets. “F”, “W” and “U” mean fully-supervised, weakly-supervised and unsupervised, respectively.

Methods	Year	Sup.	DAVSOD			DAVIS			SegV2			FBMS		
			$F_{\beta}\uparrow$	$E_{\xi}\uparrow$	$\mathcal{M}\downarrow$	$F_{\beta}\uparrow$	$E_{\xi}\uparrow$	$\mathcal{M}\downarrow$	$F_{\beta}\uparrow$	$E_{\xi}\uparrow$	$\mathcal{M}\downarrow$	$F_{\beta}\uparrow$	$E_{\xi}\uparrow$	$\mathcal{M}\downarrow$
SSAV [40]	2019	F	.540	.742	.083	.762	.902	.029	.720	.895	.024	.793	.875	.043
PCSA [45]	2020	F	.556	.749	.077	.794	.922	.022	.789	.931	.019	.783	.868	.042
TENet [46]	2020	F	.595	.773	.067	.821	.941	.017	–	–	–	.851	.915	.026
STVS [47]	2021	F	.563	.764	.080	.812	.940	.022	.835	.950	.016	.821	.903	.042
DCFNet [96]	2021	F	.599	.783	.065	.864	.964	.016	.863	.954	.013	–	–	–
WSVSOD [50]	2021	W	.492	.710	.103	.731	.900	.036	.711	.909	.031	.736	.840	.084
MM-split (Ours)	2022	U	.534	.747	.084	.751	.913	.042	.751	.914	.033	.732	.794	.100
MM-joint (Ours)	2022	U	.547	.762	.085	.756	.908	.037	.808	.927	.021	.795	.876	.060

TABLE VI: Results on RGB-T SOD datasets. “F” and “U” mean fully-supervised and unsupervised, respectively.

Methods	Year	Sup.	VT5000			VT1000			VT821		
			$F_{\beta}\uparrow$	$E_{\xi}\uparrow$	$\mathcal{M}\downarrow$	$F_{\beta}\uparrow$	$E_{\xi}\uparrow$	$\mathcal{M}\downarrow$	$F_{\beta}\uparrow$	$E_{\xi}\uparrow$	$\mathcal{M}\downarrow$
ADF [41]	2020	F	.778	.891	.048	.847	.922	.034	.717	.845	.077
MIED [48]	2020	F	.761	.880	.050	.853	.928	.030	.760	.877	.050
MIDD [49]	2021	F	.801	.899	.043	.882	.942	.027	.805	.898	.045
APNet [97]	2021	F	.821	.918	.035	.885	.951	.021	.818	.912	.034
CCFE [70]	2022	F	.859	.937	.030	.906	.963	.018	.857	.934	.027
MM-split (Ours)	2022	U	.810	.904	.046	.885	.939	.031	.805	.900	.043
MM-joint (Ours)	2022	U	.807	.903	.047	.881	.939	.032	.805	.899	.044

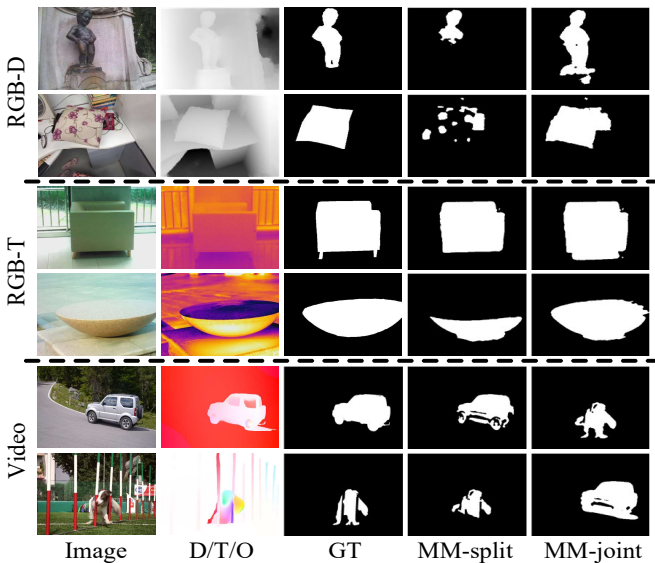


Fig. 8: Examples of the generated pseudo labels. The “D/T/O” means depth map, thermal image or optical flow.

supervised RGB-D SOD methods. For the VSOD task in Tab. V, training with our pseudo labels achieves better performance

than weakly-supervised method WSVSOD [50]. Furthermore, training on the labels of “MM-joint” reports a comparable performance against the latest fully-supervised video SOD methods. For the RGB-T SOD task in Tab. VI, training with “MM-split” achieves better results than “MM-joint” because the quality of pseudo labels is higher. In addition, their performances also are comparable to the latest fully-supervised RGB-T SOD methods.

D. Ablation Study

Comparison between Initial Saliency Cues. Existing DL-based USOD methods take advantage of traditional SOD methods and features extracted by an ImageNet pretrained network as their initial saliency cues. We evaluate the accuracy of these saliency cues on MSRA-B, as shown in Tab. VII.

In conclusion, traditional SOD methods can produce significantly more accurate saliency maps than ImageNet pretrained networks. This observation is reasonable because the pretrained networks are trained for other related vision tasks without pixel-level labels. As shown in Tab. II, most existing DL-based USOD methods [10]–[13] achieve impressive performances by integrating the prior knowledge from both traditional SOD methods and supervised pretrained networks. Different with these methods, our framework can produce

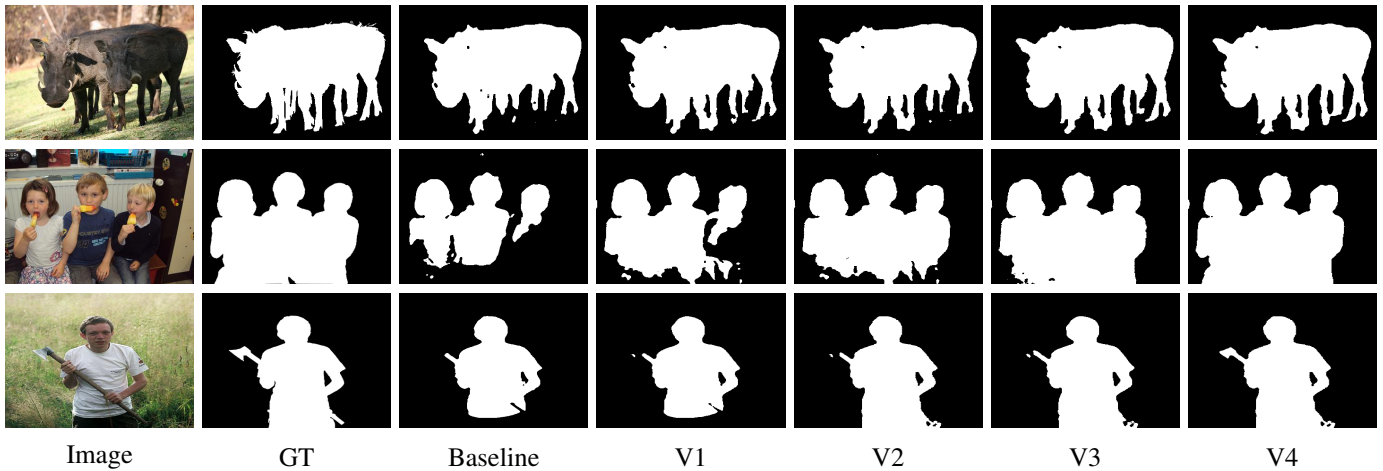


Fig. 9: Examples of the generated pseudo labels.

TABLE VII: The quality of initial saliency cues used in DL-based USOD methods. ‘‘IN-S’’ and ‘‘IN-U’’ mean supervised and unsupervised pretraining on ImageNet, respectively.

Methods	Type	$F_\beta \uparrow$	$E_\xi \uparrow$	$\mathcal{M} \downarrow$
MC [17]	Hand-crafted	.810	.877	.145
HS [14]	Hand-crafted	.774	.843	.161
DSR [15]	Hand-crafted	.780	.867	.118
RBD [16]	Hand-crafted	.803	.883	.109
IN-S [7]	DL-based	.474	.665	.321
IN-U [63]	DL-based	.451	.659	.353

TABLE VIII: Ablation study on our framework. We list the scores for the generated pseudo labels compared to human annotations in the DUTS-TR dataset.

	L_{adb}	L_{mse}	L_{aspl}	L_{agm}	Stage 2	$F_\beta \uparrow$	$E_\xi \uparrow$	$\mathcal{M} \downarrow$
Baseline	✓					.882	.915	.071
V1	✓	✓				.891	.921	.066
V2		✓	✓			.908	.937	.050
V3		✓	✓	✓		.917	.945	.038
V4		✓	✓	✓	✓	.920	.944	.037

high-quality pseudo labels by refining the saliency cues of an unsupervised pretrained network, which obtains the worst performance compared to other methods. This experiment well prove that our framework can better model the saliency in images, instead of refining multiple noisy labels as existing USOD methods.

Effectiveness of loss functions. To validate the effectiveness of each loss in the first stage, we report the scores of pseudo labels generated by different supervised signals in Tab. VIII. Compared to baseline, the scale consistency loss L_{ms} slightly improves the quality of pseudo labels. Compared to L_{adb} [18], our framework with L_{aspl} further excavates the latent saliency information, and thereby more complete objects are segmented. Furthermore, the proposed L_{agm} refines the learned saliency cues using low-level representations, which is the complete method in our first stage. Last, the results of V4 prove that the network learns the similar saliency information, but in a more generalized manner.

We also show some pseudo labels generated by these

TABLE IX: Ablation study on the proposed L_{aspl} . Several existing losses are utilized for training our saliency detector with the cooperation of L_{agm} and L_{ms} .

Loss	$F_\beta \uparrow$	$E_\xi \uparrow$	$\mathcal{M} \downarrow$
$L2$.558	.540	.208
$L1$.895	.928	.044
L_{adb} [18]	.903	.934	.042
L_{spl} [52]	.910	.938	.041
L_{aspl}	.917	.945	.038

TABLE X: Different designs of the proposed L_{agm} .

Tag	Description	$F_\beta \uparrow$	$E_\xi \uparrow$	$\mathcal{M} \downarrow$
A1	Linear appearance similarity	.735	.819	.120
A2	L_{lsc} [37]	.906	.923	.052
A3	Without boundary mask	.907	.926	.051
A4	Ours	.917	.945	.038

variants in Fig. 9. The baseline localizes salient objects but loses too many details. The pseudo labels generated by our framework are much more similar to human annotations. It proves that our framework extracts more precise saliency information from images by modeling multi-level representations.

Learning strategy comparison. Unlike supervised SOD methods, localizing salient objects in images without human annotations is challenging. We test multiple losses to validate their effectiveness on this goal, including $L2$ loss, $L1$ loss, L_{adb} [18], original L_{spl} [52] and our L_{aspl} . The results of using one of these losses to train our framework with the cooperation of L_{agm} and L_{ms} are listed in Tab. IX.

In conclusion, training with L_{aspl} loss achieves the best performance among these losses. L_{adb} and L_{spl} report lower scores than ours because they fail to learn more latent saliency information from hard samples. However, reliable saliency information in these hard samples is much less than easy samples. Therefore, $L1$ loss obtains inferior results because it pays more attention to these hard samples from the beginning. The more convincing proof is that $L2$ loss reports the worst results because our saliency generator learns saliency information mainly based on these hard samples.

Design of L_{agm} . The design of our L_{agm} loss also is crucial

TABLE XI: Effect of different hyperparameters.

Param.	Value	$F_\beta \uparrow$	$E_\xi \uparrow$	$\mathcal{M} \downarrow$	Param.	Value	$F_\beta \uparrow$	$E_\xi \uparrow$	$\mathcal{M} \downarrow$
α	100	.911	.932	.046	λ_s	0.5	.911	.937	.042
	150	.914	.937	.043		0.7	.915	.942	.039
	200	.917	.945	.038		1	.917	.945	.038
	250	.915	.942	.039		1.2	.914	.943	.038
	300	.914	.943	.039		1.5	.913	.941	.039
λ_a	0.01	.869	.915	.054	λ_m	0.5	.915	.943	.038
	0.03	.910	.938	.042		0.75	.915	.945	.038
	0.05	.917	.945	.038		1	.917	.945	.038
	0.07	.914	.945	.039		1.25	.915	.943	.039
	0.09	.908	.942	.040		1.5	.914	.941	.039

TABLE XII: Different losses for the second stage.

Loss	DUT-OMRON			ECSSD		
	$F_\beta \uparrow$	$E_\xi \uparrow$	$\mathcal{M} \downarrow$	$F_\beta \uparrow$	$E_\xi \uparrow$	$\mathcal{M} \downarrow$
BCE	.708	.834	.066	.891	.924	.047
BCE+IOU	.726	.846	.065	.894	.923	.048
BCE+IOU+SSIM	.716	.838	.067	.886	.919	.049
CTLoss	.743	.862	.061	.907	.914	.057
IOU	.745	.863	.061	.916	.938	.044

for our framework. We build some variants of L_{agm} loss: 1) We measure the appearance similarity in Eqn. 11 using the L1 distance, denoted as A_1 ; 2) We employ the appearance-guided loss L_{lsc} proposed in [37], denoted as A_2 3) We remove the boundary masks B in Eqn. 9, denoted as A_3 . All results are listed in Tab. X, including our full method A_4 .

Overall, A_4 achieves the best results among these variants. The results of A_1 demonstrate that linear distance can not effectively eliminate the impact of pixels with low similarities. A_2 and A_3 report inferior performances because edges inside the background or objects introduce noisy information into our training process.

Effect of hyperparameters. The performance of our framework is affected by several hyperparameters, including λ_s , λ_a and λ_m in Eqn. 2, as well as α in Eqn. 11. We vary these hyperparameters and exhibit their results in Tab. XI.

As the results shown, the values $\alpha = 200$, $\lambda_s = 1$, $\lambda_a = 0.05$ and $\lambda_m = 1$ work best in practice. Our framework is robust to $\alpha \in [100, 300]$, and reports the best performance for $\alpha = 200$. Moreover, our framework achieves comparable performance for various λ_s and λ_m values within $[0.5, 1.5]$. On the contrary, our framework is sensitive to λ_a . Although we observe robust performance for $\lambda_a \in [0.03, 0.07]$, λ_a outside this range (e.g., $\lambda_a = 0.01$) seems to induce significant performance drops. We attribute this performance drop to the reduced effect of pixels with highly similar appearances.

Loss for the second stage. Multiple losses have proved their effectiveness on fully-supervised SOD task, such as BCE loss [29], [30], BCE+IOU loss [83], [98], CTLoss [82], [99], BCE+IOU+SSIM loss [31]. The results of using these losses to train our saliency detector with the generated pseudo labels are exhibited in Tab. XII.

In summary, training our detector using IOU loss achieves the best results among these losses. BCE and CTLoss provide pixel-wise supervised signals, which means that training with these losses is easy to overfit the noises and thus degrade the generalization ability of our detector. Similarly, SSIM is based on regional statistics and thus is sensitive to noisy regions in pseudo labels. Unlike the above losses, IOU is robust to pixel-

level or region-level noises because it bases on global statistics.

V. CONCLUSION

In this paper, we propose an appearance-guided attentive self-paced learning framework for Unsupervised Saliency Object Detection. The proposed framework integrates both self-paced learning (SPL) and appearance guidance into a unified learning framework. Specifically, we propose an Attentive Self-Paced Learning (ASPL) paradigm that organizes the training samples in a meaningful order to excavate gradually more detailed saliency information. Moreover, we propose an Appearance Guidance Module (AGM), which formulates the local appearance contrast of each pixel as the probability of saliency boundary and finds the potential boundary of the target objects by maximizing the probability. Since the appearance can also be interpreted as the feature vector of other modalities, such as depth map, thermal image or optical flow, we further extend our framework to other multi-modality SOD tasks. Experiments on RGB, RGB-D, RGB-T, video SOD benchmarks prove that our framework achieves state-of-the-art performance against existing USOD methods and is comparable to the latest supervised SOD methods.

REFERENCES

- [1] A. Shokoufandeh, I. Marsic, and S. J. Dickinson, "View-based object recognition using saliency maps," *Image and Vision Computing*, vol. 17, no. 5-6, pp. 445–460, 1999.
- [2] C. F. Flores, A. Gonzalez-Garcia, J. van de Weijer, and B. Raducanu, "Saliency for fine-grained object recognition in domains with scarce training data," *Pattern Recognition*, vol. 94, pp. 62–73, 2019.
- [3] W. Diao, X. Sun, X. Zheng, F. Dou, H. Wang, and K. Fu, "Efficient saliency-based object detection in remote sensing images using deep belief networks," *IEEE Geoscience and Remote Sensing Letters*, vol. 13, no. 2, pp. 137–141, 2016.
- [4] P. W. Patil, S. Murala, A. Dhall, and S. Chaudhary, "Msednet: multi-scale deep saliency learning for moving object detection," in *2018 IEEE International Conference on Systems, Man, and Cybernetics (SMC)*. IEEE, 2018, pp. 1670–1675.
- [5] W. Wang, J. Shen, and F. Porikli, "Saliency-aware geodesic video object segmentation," in *Proceedings of the IEEE conference on computer vision and pattern recognition*, 2015, pp. 3395–3402.
- [6] W. Wang, J. Shen, R. Yang, and F. Porikli, "Saliency-aware video object segmentation," *IEEE transactions on pattern analysis and machine intelligence*, vol. 40, no. 1, pp. 20–33, 2017.
- [7] K. He, X. Zhang, S. Ren, and J. Sun, "Deep residual learning for image recognition," in *Proceedings of the IEEE conference on computer vision and pattern recognition*, 2016, pp. 770–778.
- [8] M. Cordts, M. Omran, S. Ramos, T. Rehfeld, M. Enzweiler, R. Benenson, U. Franke, S. Roth, and B. Schiele, "The cityscapes dataset for semantic urban scene understanding," in *Computer Vision and Pattern Recognition*, 2016.
- [9] J. Deng, W. Dong, R. Socher, L.-J. Li, K. Li, and L. Fei-Fei, "Imagenet: A large-scale hierarchical image database," in *2009 IEEE conference on computer vision and pattern recognition*. Ieee, 2009, pp. 248–255.
- [10] D. Zhang, J. Han, and Y. Zhang, "Supervision by fusion: Towards unsupervised learning of deep salient object detector," in *Proceedings of the IEEE International Conference on Computer Vision*, 2017, pp. 4048–4056.
- [11] J. Zhang, T. Zhang, Y. Dai, M. Harandi, and R. Hartley, "Deep unsupervised saliency detection: A multiple noisy labeling perspective," in *Proceedings of the IEEE conference on computer vision and pattern recognition*, 2018, pp. 9029–9038.
- [12] D. T. Nguyen, M. Dax, C. K. Mummadi, T. P. N. Ngo, T. H. P. Nguyen, Z. Lou, and T. Brox, "Deepusps: Deep robust unsupervised saliency prediction with self-supervision," *arXiv preprint arXiv:1909.13055*, 2019.
- [13] X. Lin, Z. Wu, G. Chen, G. Li, and Y. Yu, "A causal debiasing framework for unsupervised salient object detection," in *Thirty-sixth AAAI conference on artificial intelligence*, 2022.

- [14] W. Zou and N. Komodakis, "Harf: Hierarchy-associated rich features for salient object detection," in *Proceedings of the IEEE international conference on computer vision*, 2015, pp. 406–414.
- [15] X. Li, H. Lu, L. Zhang, X. Ruan, and M.-H. Yang, "Saliency detection via dense and sparse reconstruction," in *Proceedings of the IEEE international conference on computer vision*, 2013, pp. 2976–2983.
- [16] W. Zhu, S. Liang, Y. Wei, and J. Sun, "Saliency optimization from robust background detection," in *Proceedings of the IEEE conference on computer vision and pattern recognition*, 2014, pp. 2814–2821.
- [17] B. Jiang, L. Zhang, H. Lu, C. Yang, and M.-H. Yang, "Saliency detection via absorbing markov chain," in *Proceedings of the IEEE international conference on computer vision*, 2013, pp. 1665–1672.
- [18] H. Zhou, P. Chen, L. Yang, J. Lai, and X. Xie, "Activation to saliency: Forming high-quality labels for unsupervised salient object detection," *arXiv preprint arXiv:2112.03650*, 2021.
- [19] P. Krähenbühl and V. Koltun, "Efficient inference in fully connected crfs with gaussian edge potentials," *Advances in neural information processing systems*, vol. 24, pp. 109–117, 2011.
- [20] N. Liu, J. Han, and M.-H. Yang, "Picanet: Learning pixel-wise contextual attention for saliency detection," in *Proceedings of the IEEE Conference on Computer Vision and Pattern Recognition*, 2018, pp. 3089–3098.
- [21] Z. Wu, L. Su, and Q. Huang, "Cascaded partial decoder for fast and accurate salient object detection," in *Proceedings of the IEEE Conference on Computer Vision and Pattern Recognition*, 2019, pp. 3907–3916.
- [22] M. Feng, H. Lu, and E. Ding, "Attentive feedback network for boundary-aware salient object detection," in *Proceedings of the IEEE Conference on Computer Vision and Pattern Recognition*, 2019, pp. 1623–1632.
- [23] T. Wang, L. Zhang, S. Wang, H. Lu, G. Yang, X. Ruan, and A. Borji, "Detect globally, refine locally: A novel approach to saliency detection," in *Proceedings of the IEEE Conference on Computer Vision and Pattern Recognition*, 2018, pp. 3127–3135.
- [24] P. Chen, J. Lai, G. Wang, and H. Zhou, "Confidence-guided adaptive gate and dual differential enhancement for video salient object detection," in *2021 IEEE International Conference on Multimedia and Expo (ICME)*. IEEE, 2021, pp. 1–6.
- [25] W. Wang, S. Zhao, J. Shen, S. C. Hoi, and A. Borji, "Salient object detection with pyramid attention and salient edges," in *Proceedings of the IEEE Conference on Computer Vision and Pattern Recognition*, 2019, pp. 1448–1457.
- [26] X. Zhang, T. Wang, J. Qi, H. Lu, and G. Wang, "Progressive attention guided recurrent network for salient object detection," in *Proceedings of the IEEE Conference on Computer Vision and Pattern Recognition*, 2018, pp. 714–722.
- [27] P. Zhang, D. Wang, H. Lu, H. Wang, and B. Yin, "Learning uncertain convolutional features for accurate saliency detection," in *ICCV*, 2017.
- [28] O. Ronneberger, P. Fischer, and T. Brox, "U-net: Convolutional networks for biomedical image segmentation," in *International Conference on Medical image computing and computer-assisted intervention*. Springer, 2015, pp. 234–241.
- [29] P. Zhang, D. Wang, H. Lu, H. Wang, and X. Ruan, "Amulet: Aggregating multi-level convolutional features for salient object detection," in *Proceedings of the IEEE International Conference on Computer Vision*, 2017, pp. 202–211.
- [30] Q. Hou, M.-M. Cheng, X. Hu, A. Borji, Z. Tu, and P. H. Torr, "Deeply supervised salient object detection with short connections," in *Proceedings of the IEEE Conference on Computer Vision and Pattern Recognition*, 2017, pp. 3203–3212.
- [31] X. Qin, Z. Zhang, C. Huang, C. Gao, M. Dehghan, and M. Jagersand, "Basnet: Boundary-aware salient object detection," in *Proceedings of the IEEE Conference on Computer Vision and Pattern Recognition*, 2019, pp. 7479–7489.
- [32] X. Zhao, Y. Pang, L. Zhang, H. Lu, and L. Zhang, "Suppress and balance: A simple gated network for salient object detection," in *European Conference on Computer Vision*. Springer, 2020, pp. 35–51.
- [33] Y. Zeng, Y. Zhuge, H. Lu, L. Zhang, M. Qian, and Y. Yu, "Multi-source weak supervision for saliency detection," in *Proceedings of the IEEE/CVF Conference on Computer Vision and Pattern Recognition*, 2019, pp. 6074–6083.
- [34] Y. Piao, J. Wang, M. Zhang, and H. Lu, "Mfnet: Multi-filter directive network for weakly supervised salient object detection," in *Proceedings of the IEEE/CVF International Conference on Computer Vision*, 2021, pp. 4136–4145.
- [35] J. Zhang, X. Yu, A. Li, P. Song, B. Liu, and Y. Dai, "Weakly-supervised salient object detection via scribble annotations," in *Proceedings of the IEEE/CVF conference on computer vision and pattern recognition*, 2020, pp. 12 546–12 555.
- [36] L. Wang, H. Lu, Y. Wang, M. Feng, D. Wang, B. Yin, and X. Ruan, "Learning to detect salient objects with image-level supervision," in *CVPR*, 2017.
- [37] S. Yu, B. Zhang, J. Xiao, and E. G. Lim, "Structure-consistent weakly supervised salient object detection with local saliency coherence," in *Proceedings of the AAAI Conference on Artificial Intelligence (AAAI)*. AAAI Palo Alto, CA, USA, 2021.
- [38] J. Zhang, J. Xie, and N. Barnes, "Learning noise-aware encoder-decoder from noisy labels by alternating back-propagation for saliency detection," in *European conference on computer vision*. Springer, 2020, pp. 349–366.
- [39] H. Wen, C. Yan, X. Zhou, R. Cong, Y. Sun, B. Zheng, J. Zhang, Y. Bao, and G. Ding, "Dynamic selective network for rgb-d salient object detection," *IEEE Transactions on Image Processing*, vol. 30, pp. 9179–9192, 2021.
- [40] D.-P. Fan, W. Wang, M.-M. Cheng, and J. Shen, "Shifting more attention to video salient object detection," in *Proceedings of the IEEE/CVF conference on computer vision and pattern recognition*, 2019, pp. 8554–8564.
- [41] Z. Tu, Y. Ma, Z. Li, C. Li, J. Xu, and Y. Liu, "Rgbt salient object detection: A large-scale dataset and benchmark," *IEEE Transactions on Multimedia*, 2022.
- [42] P. Sun, W. Zhang, H. Wang, S. Li, and X. Li, "Deep rgb-d saliency detection with depth-sensitive attention and automatic multi-modal fusion," in *Proceedings of the IEEE/CVF conference on computer vision and pattern recognition*, 2021, pp. 1407–1417.
- [43] T. Zhou, H. Fu, G. Chen, Y. Zhou, D.-P. Fan, and L. Shao, "Specificity-preserving rgb-d saliency detection," in *Proceedings of the IEEE/CVF international conference on computer vision*, 2021, pp. 4681–4691.
- [44] X. Cheng, X. Zheng, J. Pei, H. Tang, Z. Lyu, and C. Chen, "Depth-induced gap-reducing network for rgb-d salient object detection: An interaction, guidance and refinement approach," *IEEE Transactions on Multimedia*, 2022.
- [45] Y. Gu, L. Wang, Z. Wang, Y. Liu, M.-M. Cheng, and S.-P. Lu, "Pyramid constrained self-attention network for fast video salient object detection," in *Proceedings of the AAAI conference on artificial intelligence*, vol. 34, no. 07, 2020, pp. 10 869–10 876.
- [46] S. Ren, C. Han, X. Yang, G. Han, and S. He, "Tenet: Triple excitation network for video salient object detection," in *European Conference on Computer Vision*. Springer, 2020, pp. 212–228.
- [47] C. Chen, G. Wang, C. Peng, Y. Fang, D. Zhang, and H. Qin, "Exploring rich and efficient spatial temporal interactions for real-time video salient object detection," *IEEE Transactions on Image Processing*, vol. 30, pp. 3995–4007, 2021.
- [48] Z. Tu, Z. Li, C. Li, Y. Lang, and J. Tang, "Multi-interactive encoder-decoder network for rgbt salient object detection," *arXiv e-prints*, pp. arXiv–2005, 2020.
- [49] —, "Multi-interactive dual-decoder for rgb-thermal salient object detection," *IEEE Transactions on Image Processing*, vol. 30, pp. 5678–5691, 2021.
- [50] W. Zhao, J. Zhang, L. Li, N. Barnes, N. Liu, and J. Han, "Weakly supervised video salient object detection," in *Proceedings of the IEEE/CVF conference on computer vision and pattern recognition*, 2021, pp. 16 826–16 835.
- [51] W. Ji, J. Li, Q. Bi, C. Guo, J. Liu, and L. Cheng, "Promoting saliency from depth: Deep unsupervised rgb-d saliency detection," *arXiv preprint arXiv:2205.07179*, 2022.
- [52] Y. Bengio, J. Louradour, R. Collobert, and J. Weston, "Curriculum learning," in *Proceedings of the 26th annual international conference on machine learning*, 2009, pp. 41–48.
- [53] M. Kumar, B. Packer, and D. Koller, "Self-paced learning for latent variable models," *Advances in neural information processing systems*, vol. 23, 2010.
- [54] K. Tang, V. Ramanathan, L. Fei-Fei, and D. Koller, "Shifting weights: Adapting object detectors from image to video," *Advances in Neural Information Processing Systems*, vol. 25, 2012.
- [55] L. Jiang, D. Meng, S.-I. Yu, Z. Lan, S. Shan, and A. Hauptmann, "Self-paced learning with diversity," *Advances in neural information processing systems*, vol. 27, 2014.
- [56] K. Ghasedi, X. Wang, C. Deng, and H. Huang, "Balanced self-paced learning for generative adversarial clustering network," in *Proceedings of the IEEE/CVF Conference on Computer Vision and Pattern Recognition (CVPR)*, June 2019.
- [57] P. Soviany, R. T. Ionescu, P. Rota, and N. Sebe, "Curriculum self-paced learning for cross-domain object detection," *Computer Vision and*

- Image Understanding*, vol. 204, p. 103166, 2021. [Online]. Available: <https://www.sciencedirect.com/science/article/pii/S1077314221000102>
- [58] H. Zhu, Y. Qiao, G. Xu, L. Deng, and Y.-F. Yu, "Dspnet: A lightweight dilated convolution neural networks for spectral deconvolution with self-paced learning," *IEEE Transactions on Industrial Informatics*, vol. 16, no. 12, pp. 7392–7401, 2019.
- [59] D. Zhang, D. Meng, and J. Han, "Co-saliency detection via a self-paced multiple-instance learning framework," *IEEE Transactions on Pattern Analysis and Machine Intelligence*, vol. 39, no. 5, pp. 865–878, 2017.
- [60] R. Achanta, A. Shaji, K. Smith, A. Lucchi, P. Fua, and S. Süsstrunk, "Slic superpixels compared to state-of-the-art superpixel methods," *IEEE transactions on pattern analysis and machine intelligence*, vol. 34, no. 11, pp. 2274–2282, 2012.
- [61] V. Kwatra, A. Schödl, I. Essa, G. Turk, and A. Bobick, "Graphcut textures: Image and video synthesis using graph cuts," *Acm transactions on graphics (tog)*, vol. 22, no. 3, pp. 277–286, 2003.
- [62] C. Tomasi and R. Manduchi, "Bilateral filtering for gray and color images," in *Sixth international conference on computer vision (IEEE Cat. No. 98CH36271)*. IEEE, 1998, pp. 839–846.
- [63] X. Chen, H. Fan, R. Girshick, and K. He, "Improved baselines with momentum contrastive learning," *arXiv preprint arXiv:2003.04297*, 2020.
- [64] A. Paszke, S. Gross, S. Chintala, G. Chanan, E. Yang, Z. DeVito, Z. Lin, A. Desmaison, L. Antiga, and A. Lerer, "Automatic differentiation in pytorch," in *NIPS Workshops*, 2017.
- [65] T. Liu, Z. Yuan, J. Sun, J. Wang, N. Zheng, X. Tang, and H.-Y. Shum, "Learning to detect a salient object," *IEEE Transactions on Pattern Analysis and Machine Intelligence*, vol. 33, no. 2, pp. 353–367, 2010.
- [66] J. Shi, Q. Yan, L. Xu, and J. Jia, "Hierarchical image saliency detection on extended cssd," *IEEE transactions on pattern analysis and machine intelligence*, vol. 38, no. 4, pp. 717–729, 2015.
- [67] Y. Li, X. Hou, C. Koch, J. M. Rehg, and A. L. Yuille, "The secrets of salient object segmentation," in *CVPR*, 2014.
- [68] G. Li and Y. Yu, "Visual saliency based on multiscale deep features," in *CVPR*, 2015.
- [69] C. Yang, L. Zhang, H. Lu, X. Ruan, and M.-H. Yang, "Saliency detection via graph-based manifold ranking," in *CVPR*, 2013.
- [70] G. Liao, W. Gao, G. Li, J. Wang, and S. Kwong, "Cross-collaborative fusion-encoder network for robust rgb-thermal salient object detection," *IEEE Transactions on Circuits and Systems for Video Technology*, 2022.
- [71] H. Peng, B. Li, W. Xiong, W. Hu, and R. Ji, "Rgbd salient object detection: A benchmark and algorithms," in *European conference on computer vision*. Springer, 2014, pp. 92–109.
- [72] R. Ju, L. Ge, W. Geng, T. Ren, and G. Wu, "Depth saliency based on anisotropic center-surround difference," in *2014 IEEE international conference on image processing (ICIP)*. IEEE, 2014, pp. 1115–1119.
- [73] Y. Cheng, H. Fu, X. Wei, J. Xiao, and X. Cao, "Depth enhanced saliency detection method," in *Proceedings of international conference on internet multimedia computing and service*, 2014, pp. 23–27.
- [74] D.-P. Fan, Z. Lin, Z. Zhang, M. Zhu, and M.-M. Cheng, "Rethinking rgb-d salient object detection: Models, data sets, and large-scale benchmarks," *IEEE Transactions on neural networks and learning systems*, vol. 32, no. 5, pp. 2075–2089, 2020.
- [75] Z. Tu, Y. Ma, Z. Li, C. Li, J. Xu, and Y. Liu, "Rgbd salient object detection: A large-scale dataset and benchmark," *IEEE Transactions on Multimedia*, 2022.
- [76] Z. Tu, T. Xia, C. Li, X. Wang, Y. Ma, and J. Tang, "Rgb-t image saliency detection via collaborative graph learning," *IEEE Transactions on Multimedia*, vol. 22, no. 1, pp. 160–173, 2019.
- [77] G. Wang, C. Li, Y. Ma, A. Zheng, J. Tang, and B. Luo, "Rgb-t saliency detection benchmark: Dataset, baselines, analysis and a novel approach," in *Chinese Conference on Image and Graphics Technologies*. Springer, 2018, pp. 359–369.
- [78] F. Perazzi, J. Pont-Tuset, B. McWilliams, L. Van Gool, M. Gross, and A. Sorkine-Hornung, "A benchmark dataset and evaluation methodology for video object segmentation," in *Proceedings of the IEEE conference on computer vision and pattern recognition*, 2016, pp. 724–732.
- [79] F. Li, T. Kim, A. Humayun, D. Tsai, and J. M. Rehg, "Video segmentation by tracking many figure-ground segments," in *Proceedings of the IEEE international conference on computer vision*, 2013, pp. 2192–2199.
- [80] T. Brox and J. Malik, "Object segmentation by long term analysis of point trajectories," in *European conference on computer vision*. Springer, 2010, pp. 282–295.
- [81] Z. Wu, L. Su, and Q. Huang, "Stacked cross refinement network for edge-aware salient object detection," in *Proceedings of the IEEE International Conference on Computer Vision*, 2019, pp. 7264–7273.
- [82] H. Zhou, X. Xie, J.-H. Lai, Z. Chen, and L. Yang, "Interactive two-stream decoder for accurate and fast saliency detection," in *Proceedings of the IEEE/CVF Conference on Computer Vision and Pattern Recognition*, 2020, pp. 9141–9150.
- [83] Y. Pang, X. Zhao, L. Zhang, and H. Lu, "Multi-scale interactive network for salient object detection," in *Proceedings of the IEEE/CVF Conference on Computer Vision and Pattern Recognition*, 2020, pp. 9413–9422.
- [84] J. Wei, S. Wang, Z. Wu, C. Su, Q. Huang, and Q. Tian, "Label decoupling framework for salient object detection," in *Proceedings of the IEEE/CVF Conference on Computer Vision and Pattern Recognition*, 2020, pp. 13 025–13 034.
- [85] B. Xu, H. Liang, R. Liang, and P. Chen, "Locate globally, segment locally: A progressive architecture with knowledge review network for salient object detection," in *Proceedings of the AAAI Conference On Artificial Intelligence*, 2021, pp. 1–9.
- [86] L. Wang, H. Lu, Y. Wang, M. Feng, D. Wang, B. Yin, and X. Ruan, "Learning to detect salient objects with image-level supervision," in *Proceedings of the IEEE conference on computer vision and pattern recognition*, 2017, pp. 136–145.
- [87] G. Li, Y. Xie, and L. Lin, "Weakly supervised salient object detection using image labels," in *Thirty-second AAAI conference on artificial intelligence*, 2018.
- [88] C. Yang, L. Zhang, H. Lu, X. Ruan, and M.-H. Yang, "Saliency detection via graph-based manifold ranking," in *Proceedings of the IEEE conference on computer vision and pattern recognition*, 2013, pp. 3166–3173.
- [89] Y. Wei, F. Wen, W. Zhu, and J. Sun, "Geodesic saliency using background priors," in *European conference on computer vision*. Springer, 2012, pp. 29–42.
- [90] J. Zhang, S. Sclaroff, Z. Lin, X. Shen, B. Price, and R. Mech, "Minimum barrier salient object detection at 80 fps," in *Proceedings of the IEEE international conference on computer vision*, 2015, pp. 1404–1412.
- [91] J. Zhang and S. Sclaroff, "Saliency detection: A boolean map approach," in *Proceedings of the IEEE international conference on computer vision*, 2013, pp. 153–160.
- [92] Q. Yan, L. Xu, J. Shi, and J. Jia, "Hierarchical saliency detection," in *Proceedings of the IEEE conference on computer vision and pattern recognition*, 2013, pp. 1155–1162.
- [93] R. Achanta, S. Hemami, F. Estrada, and S. Susstrunk, "Frequency-tuned salient region detection," in *2009 IEEE conference on computer vision and pattern recognition*. IEEE, 2009, pp. 1597–1604.
- [94] D.-P. Fan, C. Gong, Y. Cao, B. Ren, M.-M. Cheng, and A. Borji, "Enhanced-alignment Measure for Binary Foreground Map Evaluation," in *International Joint Conference on Artificial Intelligence (IJCAI)*, 2018, pp. 698–704, <http://dpfan.net/e-measure/>.
- [95] K. Simonyan and A. Zisserman, "Very deep convolutional networks for large-scale image recognition," *arXiv preprint arXiv:1409.1556*, 2014.
- [96] M. Zhang, J. Liu, Y. Wang, Y. Piao, S. Yao, W. Ji, J. Li, H. Lu, and Z. Luo, "Dynamic context-sensitive filtering network for video salient object detection," in *Proceedings of the IEEE/CVF International Conference on Computer Vision*, 2021, pp. 1553–1563.
- [97] W. Zhou, Y. Zhu, J. Lei, J. Wan, and L. Yu, "Apnet: Adversarial learning assistance and perceived importance fusion network for all-day rgb-t salient object detection," *IEEE Transactions on Emerging Topics in Computational Intelligence*, 2021.
- [98] J.-X. Zhao, J.-J. Liu, D.-P. Fan, Y. Cao, J. Yang, and M.-M. Cheng, "Egnet: Edge guidance network for salient object detection," in *Proceedings of the IEEE International Conference on Computer Vision*, 2019, pp. 8779–8788.
- [99] Z. Chen, H. Zhou, X. Xie, and J. Lai, "Contour loss: Boundary-aware learning for salient object segmentation," *arXiv preprint arXiv:1908.01975*, 2019.